Applied Catalysis B: Environmental 179 (2015) 262–275

Contents lists available at ScienceDirect

Applied Catalysis B: Environmental

journal homepage: www.elsevier.com/locate/apcatb

Hydrogen production by methanol steam reforming: Catalytic performance of supported-Pd on zinc–cerium oxides' nanocomposites

Celina E. Barrios, Marta V. Bosco, Miguel A. Baltanás*, Adrian L. Bonivardi

Instituto de Desarrollo Tecnológico para la Industria Química (Universidad Nacional del Litoral and CONICET), Güemes 3450, 3000 Santa Fe, Argentina

ARTICLE INFO

Article history:
Received 22 October 2014
Received in revised form 10 April 2015
Accepted 12 May 2015
Available online 14 May 2015

Keywords:
Fuel cells
Palladium dispersion
Palladium–zinc intermetallic
Clean energy

ABSTRACT

Two series of supported palladium catalysts (2 wt%) were prepared on ZnO–CeO_2 nanocomposites (Zn-to-Ce atomic ratio between 0.5 and 2) obtained by oxalate or carbonate coprecipitation (OC and CC series, respectively). Methanol steam reforming (MSR) reaction was tested in a wide range of temperature (398–623 K) for CH_3OH/H_2O = 1/1 gas mixtures. Pd on pure CeO_2 was only able to decompose methanol to CO, under 523 K, but the reverse water gas shift reaction took place at higher temperatures. The MSR reaction only occurred in the presence of zinc oxide and the selectivity to CO_2 was higher for the CC series, due to the better dispersion of the ZnO phase over these carbonate-derived nanocomposites. Although the CO_2 selectivity seems to be modulated by the reverse water gas shift reaction, the palladium supported on the mixed oxides was more stable than Pd/ZnO, which continuously deactivated. A detailed characterization by high resolution atomic microscopy, X-ray photoelectron spectroscopy and a novel carbon monoxide step chemisorption technique, proved the formation of bulk and surface PdZn alloying in the ternary catalyst, Pd supported on the nanosized ceria and zinc oxide supports. It is concluded that although a better catalytic stability was observed on the ZnO–CeO_2 nanocomposites, the employment of temperatures higher than 450 K would impose an insurmountable limitation in terms of CO_2 selectivity.

1. Introduction

Polymeric electrolyte membrane fuel cells (PMEFCs) have emerged as an important technological alternative to supply "clean" energy to various devices, by feeding the cells with molecular hydrogen [1]. Said H_2 stream must meet several specifications, though, some of which are a low concentration level of CO (less than 20 ppm) to avoid Pt anode poisoning of the PMEFC and a stable H_2 production, preferentially from an organic liquid source able to store hydrogen in a high energy-to-volume ratio. Thus, the production of H_2 by the methanol steam reforming (MSR) has been envisaged as a promising alternative [1,2]. Even if a further purification of the H_2 stream is unavoidable to fit the PMEFC's requirements, one of the aims of a MSR based process is to decrease in as much as possible the amount of CO at the exit, which can be produced by the concurrent methanol decomposition (MD) and/or the reverse water gas shift (RWGS) reaction. Whichever the CO purification process that may be chosen (e.g., from an uncoupled WGS unit to a coupled Pd membrane reactor working at low or high temperature, respectively [3]), only two of the previous reactions are needed to fully predict the equilibrium thermodynamic composition, and the general conclusion is that a low reaction temperature is beneficial to prevent the MD and/or RWGS reactions which proceed together with the MSR reaction or, in other words, to maximize the selectivity to CO_2 at the expense of CO.

Among the lot of catalysts tested for the MSR reaction, those based on palladium alloys (or intermetallics), mainly PdZn alloys, have emerged as the most promising ones [2,4] due to their renowned selectivity to carbon dioxide. Iwasa et al. were the first to compare a series of Pd-supported Zn-modified catalysts over a wide variety of oxides (ZnO, SiO_2, Al_2O_3, Pr_6O_{11}, MgO, ZrO_2, CeO_2) and carbon [5]. Both, the low surface area of pure ZnO and the poor stability of Pd/ZnO were the driving forces for the use of some other supports. In this regard, Al_2O_3 and Y-modified CeO_2, as supports of the palladium-zinc system, have been examined in the literature with some degree of success [3,6–10]. However, it is not yet clear whether the first one is able to provide a good stability while the second one, though with better performance, deserves a closer look to its intrinsic behavior.

Therefore, we set up a systematic experimental program to improve the understanding of the Pd–ZnO–CeO_2 system. The detailed preparation and characterization of two different series of ZnO–CeO_2 nanocomposites – free of any other residual ion rather than zinc(II) and cerium(IV)-, as supports, were already reported by

* Corresponding author. Tel.: +54 342 4559175; fax: +54 342 4550944.
E-mail address: tderliq@santafe-conicet.gov.ar (M.A. Baltanás).

http://dx.doi.org/10.1016/j.apcatb.2015.05.030
0926-3373/

Table 1
Morphological properties of selected supports and catalysts.

Material	Abridged designation	S_{BET}[a] ($m^2\ g^{-1}$)	V_p[b] ($cm^3\ g^{-1}$)	d_p[c] (nm)
Supports[d]				
CC–Ce	CeO_2	83	0.05	4
CC–ZnCe05 (Zn/Ce = 0.5 at/at)	ZnO–CeO_2	63	0.05	14
IO–ZnCe04 (nominal ZnO coverage = 0.4)	ZnO/CeO_2	52	0.08	6
CC–Zn	ZnO	8	0.06	38
Catalysts				
(2 wt%) Pd/CeO_2	Pd/CeO_2	80	0.04	1.3
(2 wt%) Pd/ZnO–CeO_2	Pd/ZnO–CeO_2	50	0.015	1.3
(1 wt%) Pd/ZnO/CeO_2	Pd/ZnO/CeO_2	52	0.015	1.2
(2 wt%) Pd/ZnO	Pd/ZnO	8	0.002	1.4
(2 wt%) Pd/SiO_2[e]	Pd/SiO_2	301		8.0

[a] BET (LN_2) specific surface.
[b] Pore volume.
[c] Barrett–Joyner–Halenda (BJH) pore diameter.
[d] CC: carbonate (co) precipitation; IO: ZnO impregnated ceria (ex-oxalate).
[e] Davison Grade 59.

some of us [11]. Thus, the strategy here was to maximize surface area, metal dispersion and – hopefully- improve the catalytic activity of the only active Pd/ZnO/Y-CeO_2 reported catalyst [3,9,10] so as to be able to operate the MSR reaction at lower temperature while preserving the bimetallic PdZn surface-alloyed formation, which is claimed to be essential to keep high CO_2 selectivity values. In this work, we present the catalytic performance of the whole set of Pd-based catalysts over those supports under MSR conditions, including an in-depth characterization by means of high resolution electron microscopy, X-ray photoelectron spectroscopy and CO chemisorption by a step method developed to avoid CO chemisorption and/or spillover on the ceria surface, by introducing a steady, low concentration of CO_2 in the gas stream.

2. Experimental

2.1. Catalysts

A set of supported Pd catalysts was prepared by incipient wetness impregnation, at room temperature, of acetone-diluted $Pd(AcO)_2$ (Sigma 99.97% Pd) onto pure zinc(II) and cerium(IV) oxides, as well as *composites* of both oxides containing different Zn/Ce = 0.5, 1 and 2 at/at ratios. The supports were synthesized using two alternate co-precipitation routes designated as OC (oxalates coprecipitation) and CC (carbonates coprecipitation), with further drying and calcining in each case. The obtained materials were labeled indicating the preparation method (OC or CC), metal cation(s) and/or Zn/Ce atomic ratio (Ce, Zn, ZnCe). For comparison purposes – and economic reasons as well-, a third (conventional) type of composite support, in which ZnO was incorporated onto ceria (ex-oxalate, that is, derived from the oxalate precursor) by incipient wetness, was also included. In this last case, two different ZnO nominal coverages were used (θ = 0.4 and 1), which correspond to 3.5 and 11 wt% ZnO loadings, and were designated as IO–CeZn04 and IO–CeZn1, respectively.

Approximately 2 wt% Pd was added to the OC and CC support series, while only 1 wt% Pd was incorporated to the IO supports instead. After vacuum drying (333 K, 2 h), the impregnated precursors were calcined in a glass reactor using synthetic air (from 298 to 673 K with β = 3 K min^{-1}) at 673 K for 2 h. The materials were then crushed and sieved, keeping the 40/80 mesh fraction, and stored in a dessicator, prior to their use. Table 1 contains appropriate structural information about a representative sub-set of these supports and catalysts. Detailed characterization data about the complete set is given elsewhere [11].

For comparison purposes, a reference (2 wt%) Pd/SiO_2 catalyst, obtained by ion exchanging $Pd(AcO)_2$ on SiO_2 (Davison 59, S_{BET} = 301 $nm^2\ g^{-1}$) at pH 11, in NH_4OH(aq) [12] was also included in the experimental program.

2.2. Equipment

The evaluation of catalytic performance was made at atmospheric pressure, using a thermostatized glass-lined stainless steel microrreactor (length: 65 mm, I.D.: 3.5 mm). An equimolar mixture of the liquid reactants, CH_3OH/H_2O, together with a stream of helium diluent, was continuously fed to an evaporator (operated at 393 K), using a Sage 220 syringe pump. Downstream, tubing and valves were heated, also at 393 K, to prevent condensation.

Two Shimadzu 9A gas chromatographs (GC1 and GC2) were used in parallel, with a 6-way sampling valve, to measure the gas composition at the inlet and exit of the reactor. Water and carbon dioxide (TCD) and methanol, methane and methyl formate (FID) were quantified on GC1 using a Porapak Q packed column and He as carrier gas. Carbon monoxide, carbon dioxide and methane (TCD) were measured on GC2 using a Carbosieve II column and H_2 as carrier gas. A glass condensator (273 K) was placed before the sampling valve of GC2 to collect and separate liquid products.

2.3. Catalysts performance experiments

In a typical run, 50 mg of powdered catalyst (40/60 mesh), diluted 1:5 with fine quartz grains (80/100 mesh) was placed into the reactor, between two layers (~2 cm/ea.) of silanized quartz wool. For MSR evaluation, 50 $cm^3{}_{NTP}\ min^{-1}$ He were passed through the vaporizer, so as to feed the equimolar CH_3OH/H_2O mixture to the reactor (8 v/v% of each reactant). The gas hourly space velocity (GHSV) was 71,500 $cm^3\ h^{-1}\ g^{-1}$ and the $W/F^0{}_{CH3OH}$ ratio was 174 g h $m^{-3}{}_{CH3OH}$.

Each catalyst was prereduced in situ under pure H_2 (50 $cm^3{}_{NTP}\ min^{-1}$) by heating from 298 to 623 K (β = 2 K min^{-1}) and keeping this last temperature during 2 h. The reactor was then cooled to 398 K and the gas stream was switched to pure He (50 $cm^3{}_{NTP}\ min^{-1}$). After 30 min, the mixture of helium diluted, vaporized reactants was fed to the reactor.

This pretreatment was chosen to ensure the formation of a PdZn alloy (wherever applicable [7,13–27]) prior to evaluating the catalysts' performance. The MSR study was done using 'temperature steps', from 398 to 623 K (1 h/ea.; β = 1 K min^{-1} between steps), and progressively cooling, also stepwise, afterwards.

Additional runs were made with selected catalysts (2 wt%) Pd/CC–Ce, (2 wt%) Pd/CC–Zn, (2 wt%) Pd/CC–ZnCe05 and (1 wt%)

Pd/IO–ZnCe04, to assess: (i) their catalytic stability in the MSR of the He diluted equimolar CH_3OH/H_2O mixture, and (ii) their behavior in methanol decomposition, using 6.5 v/v% CH_3OH in He (GHSV = 64,200 $cm^3\ g^{-1}\ h^{-1}$; W/F^0_{CH3OH} = 240 g h m^{-3}_{MetOH}). Fresh samples of each material were used in every case.

Percent reactants conversion (X_i) and carbon-based product selectivities (S_i) were defined as:

$$\chi_i = \frac{F_i^0 - F_i}{F_i^0} \times 100(\%) \quad (1)$$

$$S_{CO_2} = \frac{y_{CO_2}}{(y_{CO_2} + y_{CO})} \times 100(\%) \quad (2)$$

$$S_{CO} = \frac{y_{CO}}{(y_{CO_2} + y_{CO})} \times 100(\%) \quad (3)$$

where y_{CO} and y_{CO2} are molar fractions at the reactor exit, and $F_i{}^0$ and F_i are inlet and exit molar flow rates of the *i*-th reactant. Within the framework of the gas chromatography technique (that is, with a ≥97% precision) the carbon balance was duly satisfied, as the combined molar fractions of CO and CO_2 entirely matched the conversion of methanol.

2.4. Surface-exposed fraction (SEF) of palladium

As indicated in the Introduction section, the determination of the surface-exposed fraction (SEF) of metals supported on ceria by CO chemisorption is by no means straightforward. So, an experimental protocol and measuring device was designed, and validated using well-characterized (2 wt%) Pd/SiO_2 [12] and (3 wt%) $Pt/Ce_{0.68}Zr_{0.32}O_2$ [29] benchmark catalysts, by comparing our step CO chemisorption data, obtained using a novel technique detailed below, and TEM information given in said references. The second material was deliberately chosen because it is a catalyst for which CO spillover is known to occur at room temperature (RT). CO chemisorption was made at RT in a glass-lined plug flow stainless steel microreactor (I.D.: 3.5 mm), using a TCD detector. Samples of selected, representative catalysts (50 or 100 mg/ea.) were diluted 1:3 with quartz (40/80 mesh). The catalysts were pretreated in situ under H_2 flow (50 $cm^3\ min^{-1}$) from RT up to the designated reduction temperature (423, 474, 523 or 623 K), heating at 5 K/min and holding for 1 h. Then, pure He was passed at 623 K (30 min), cooling under flow down to RT. Next, the catalyst was exposed to a mixture of CO_2(1%)/He during 1 h (20 $cm^3\ min^{-1}$) and the TCD signal was zeroed. Then, a second stream of dilute CO(1%)/He (1 $cm^3\ min^{-1}$) was added. The resulting composition of the ternary chemisorption mixture was CO(0.047%)/CO_2(0.95%)/He (total flow rate: 21 $cm^3\ min^{-1}$).

The partial pressure of CO_2 during the saturation stage was 8.4 Torr, whereas during the CO chemisorption step the partial pressures were p_{CO2} = 7.9 and p_{CO} = 0.4 Torr, respectively. The partial pressure of CO_2 was selected to ensure the complete saturation of the supports during the run, which was previously verified for every material by means of standard (double isotherm) stepwise static chemisorption of CO_2, using a Micromeritics ASAP 2000 unit. Under these CO_2 surface-saturating conditions CO spillover becomes almost entirely minimized (See Supplementary information). The amount of sorbed CO was computed by measuring the elapsed time between the initial switching of the CO/He stream and the breakthrough time signal (at mid value), multiplying by the molar flow rate of CO. The surface exposed metal fraction was calculated assuming a stoichiometric CO:Pd_s = 1:1 at/at ratio (Pd_s = superficial palladium).

2.5. Electron microscopy

High resolution transmission electron microscopy (HRTEM) images were obtained using a STEM unit (JEOL, model JEM-2010 FasTEM) equipped with Gatan image filters and high-angle annular dark-field (HAADF) capabilities. The catalyst powders were deposited on a copper sample holder, by dispersing them with ethanol.

The samples were pretreated ex-situ in flowing H_2 (50 $cm^3\ min^{-1}$) at 423 or 623 K (β = 2 K min^{-1}), holding 1 h. Then, He (50 $cm^3\ min^{-1}$) was passed, at 623 K (15 min), cooling afterwards under flow. Once RT was reached, the pretreatment chamber was swept with 150 $cm^3\ min^{-1}$ N_2 (INDURA, 99.998%, 10 ppm O_2) for 1 h. Finally, the oxygen concentration was raised to 50 ppm, by incorporating a standard O_2(1%)/He mixture to the nitrogen for 45 min, after which the catalysts were exposed to the atmosphere. The reduced and passivated catalysts were stored in a dessicator prior to microscopic examination. HRTEM and HAADF images of unreduced samples of Pd/SiO_2, Pd/CeO_2 and Pd/ZnO (calcined at 673 K) were also included in the analyses.

2.6. X-ray photoelectron spectroscopy (XPS)

The XPS measurements were carried out using a multitechnique system (SPECS) equipped with a dual Mg/Al X-ray source and a hemispherical PHOIBOS 150 analyzer, operating in the fixed analyzer transmission (FAT) mode. The spectra were obtained using the Al-Kα X-ray source operated at 200 W and 12 kV, with pass energy of 30 eV. The working pressure in the analyzing chamber was less than 2×10^{-8} Pa. The XPS analyses were performed on finely ground samples of the catalysts, using a metallic sample holder. Each sample was treated in situ in a pretreatment chamber attached to the main XPS chamber by calcining at 623 K in O_2 (5%)/Ar flow for 10 min (β = 10 K min^{-1}) with subsequent reduction at 423 K and 623 K in H_2 (5%)/Ar flow, for 10 min each time (β = 10 K min^{-1}). For simplicity, these treatments will be labeled as: (1) O_2-623, (2) H_2-423 and (3) H_2-623 herein after. After each treatment, the samples were degassed and directly transferred to the analysis chamber without exposure to air. The spectral regions corresponding to Ce 3d, C 1s, O 1s, Pd 3d, Zn 2p core levels and Zn LMM Auger signals were recorded. All photoelectron binding energies were referenced to the C 1s peak of adventitious carbon, set at 285 eV.

The data treatment was performed with the Casa XPS program (Casa Software Ltd., UK). The peak areas were determined by integration employing a Shirley-type background. Peaks were considered to be a mixture of Gaussian and Lorentzian functions in a 70/30 ratio. For the quantification of the elements, sensitivity factors provided by the manufacturer were used.

2.7. Gases and reagents

For the reaction experiments, He (99.999%) and H_2 (99.998%) supplied by Indura (Air Products Argentina) were used as received. For the SEF determinations, ultra high purity He, N_2 and H_2 (99.999%), together with CO (AGA, research grade, 99.99%) and CO_2 (AGA, 99.996%) were used. Oxygen and water impurities were removed with MnO/Al_2O_3 and molecular sieve (3 Å, Fisher Co) traps, respectively. Calibrated CO(1%)/He and CO_2(1%)/He mixtures were also used. Methanol (Merck) purity was 99.9%; water was tridistilled (>16.3 MΩ).

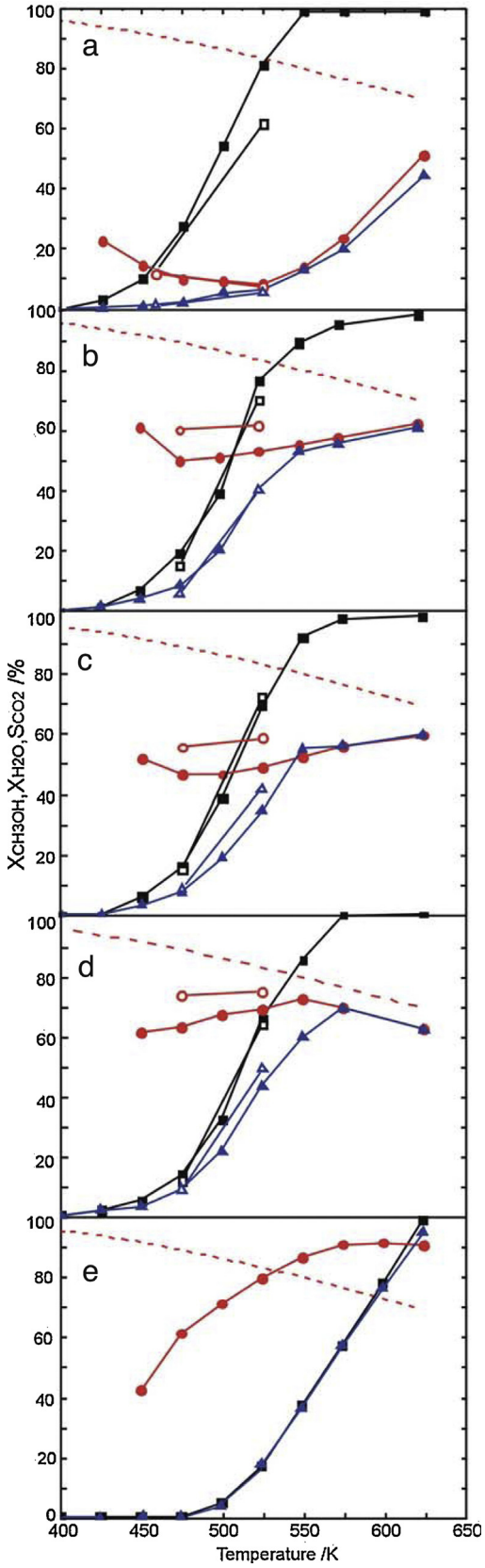

Fig. 1. Percent methanol and water conversions, X_{CH3OH} (black) and X_{H2O} (blue), and percent selectivity to carbon dioxide, S_{CO2} (red), vs. temperature on (a) Pd/OC–Ce, (b) Pd/OC–ZnCe05, (c) Pd/OC–ZnCe1, (d) Pd/OC–ZnCe2 and (e) Pd/OC–Zn. The dashed line corresponds to the calculated value of percent S_{CO2} at thermodynamic equilibrium. Filled symbols: upon increasing temperature; open symbols: upon decreasing temperature. Process conditions: $P = 0.1$ MPa; $CH_3OH/H_2O/He = 8/8/84$ v/v%; GHSV = 71,500 $cm^3\ h^{-1}\ g^{-1}$; $W/F^0_{CH3OH} = 174\ g\ h\ m^{-3}{}_{CH3OH}$. (For interpretation of the references to color in this figure legend, the reader is referred to the web version of this article.)

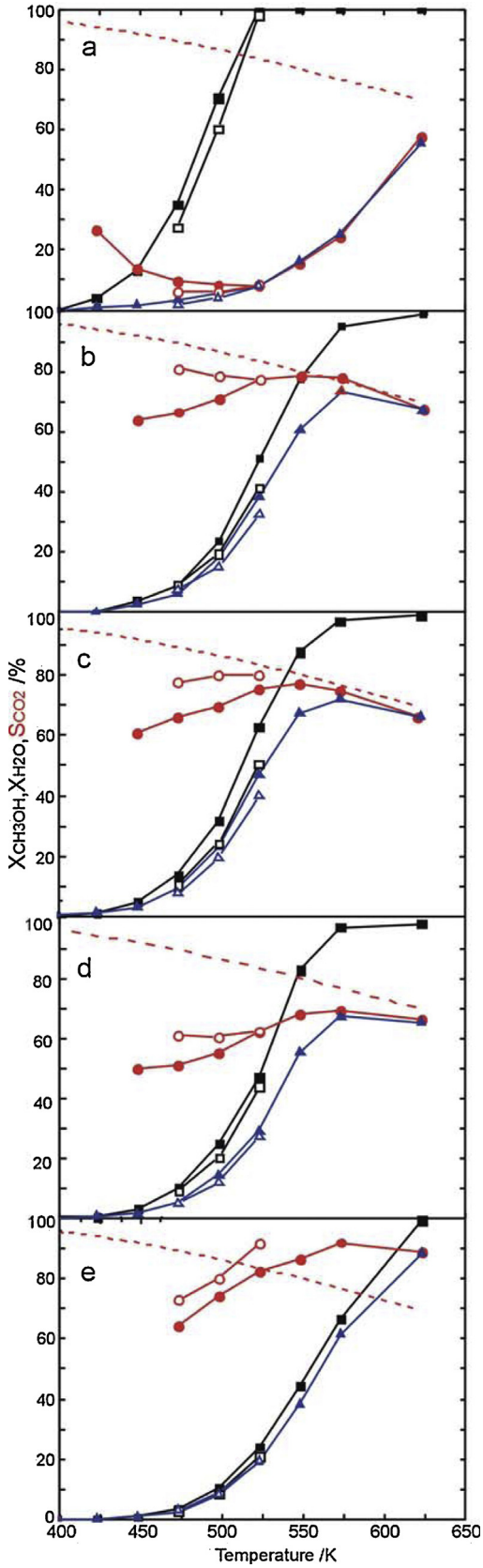

Fig. 2. Percent methanol and water conversions, X_{CH3OH} (black) and X_{H2O} (blue), and percent selectivity to carbon dioxide, S_{CO2} (red), vs. temperature on (a) Pd/CC–Ce, (b) Pd/CC–ZnCe05, (c) Pd/CC–ZnCe1, (d) Pd/CC–ZnCe2 and (e) Pd/CC–Zn. Process conditions and symbols as indicated in Fig. 1. (For interpretation of the references to color in this figure legend, the reader is referred to the web version of this article.)

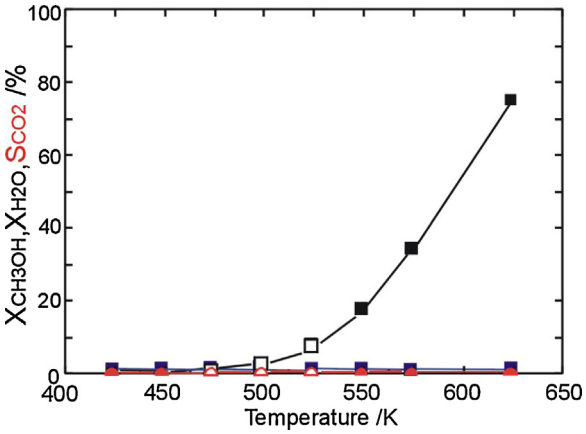

Fig. 3. Percent methanol and water conversions, X_{CH3OH} (black) and X_{H2O} (blue), and percent selectivity to carbon dioxide, S_{CO2} (red), vs. temperature on the reference catalyst, 2 wt% Pd/SiO_2. Process conditions and symbols as indicated in Fig. 1. (For interpretation of the references to color in this figure legend, the reader is referred to the web version of this article.)

3. Results

3.1. Catalysts performance

Figs. 1 and 2 show methanol and water conversions vs. reaction temperature, together with selectivity to carbon dioxide (S_{CO2}), of each of the supported Pd catalysts of the OC and CC series, respectively. The pure supports, CeO_2 and ZnO (as well as silica), were completely inactive under these reaction conditions.

The Pd/CeO_2 catalysts (Pd/OC–Ce and Pd/CC–Ce) showed a similar behavior, reaching 100% methanol conversion at about 523–548 K. However, water conversion was extremely low (e.g., X_{H2O} ~7%, at 523 K) and S_{CO2} was below 25% under 523 K and increased, steadily, above said temperature to reach aprox. 55% at 623 K (close to the thermodynamic equilibrium value, S_{CO2}^{eq} = 70% – dashed lines-). This increase was accompanied by higher X_{H2O}. Combined results suggest that methanol decomposition (MD) prevails on these catalysts, whereas in the high temperature region (T > 523 K) the water gas shift (WGS) reaction progressively sets in. These inferences are directly indicated by the stoichiometry of the related reactions, namely:

$$CH_3OH + H_2O \; <-> \; H_2 + CO_2 \qquad \text{MSR}$$

$$CH_3OH \; <--> \; CO + 2H_2 \qquad \text{MD}$$

$$CO + H_2O \; <--> \; CO_2 + H_2 \qquad \text{WGS}$$

Water conversion was negligible on the 2 wt% Pd/SiO_2 catalyst throughout the entire temperature range, even at 623 K, where methanol conversion reached 80% (Fig. 3). The only measurable product was CO (S_{CO2} = 0%), which indicates that only MD took place on this catalyst.

These results are consistent with Takezawa and Iwasa's studies of the MSR and MD reactions on transition metals: only the last reaction was observed when Pd was supported onto SiO_2 (an inert, non-reducible support), generating CO even at 493 K, when the reactor was fed with an equimolar CH_3OH/H_2O mixture, indicating that methanol decomposition was the only reaction taking place, on the disperse Pd crystallites [30].

Given that the Pd loading was the same on the Pd/SiO_2 and the Pd/CeO_2 catalysts, that the surface-exposed fraction (SEF) of the metallic particles was about twice on the former one (44 vs. 25%, see below), and that both pure supports were inactive, it is logical to attribute the higher activity observed on the Pd/CeO_2 catalysts to the presence of an 'active' metal-support interaction (or interface?), which is – at least – responsible of favoring the WGS reaction and (eventually, also) methanol decomposition.

Finally, the reactants conversion and S_{CO2} values were very similar on both Pd/CeO_2 catalysts in the descending temperature steps as compared to the values recorded in the ascending steps, which suggests that the catalysts' pretreatment was adequate to give stable materials within the temperature range used in this study, and under the joint presence of methanol and water.

The performance of both Pd/ZnO catalysts (Pd/OC–Zn and Pd/CC–Zn) toward the MSR reaction was also quite similar (Figs. 1 and 2e): X_{CH3OH} and X_{H2O} increased alongside the higher the reaction temperature was, but the latter became (slightly) smaller with heating. The selectivity to CO_2 was above 65%, also increasing with temperature. These results indicate that MSR frankly prevails on these catalysts (rather than the alternate, coupled MD + WGS route): From 523 K upward S_{CO2} was above the thermodynamic equilibrium values, which would not be feasible if the MD + WGS reaction pathway was operating instead. Furthermore, it is also apparent that the reverse water gas shift reaction (RWGS) is kinetically constrained as well.

This outstanding selectivity to CO_2 suggests that on the Pd/ZnO catalysts the surface Pd atoms are (mostly) isolated or far apart enough on the metallic crystallite surface, most likely due to the formation of a "full 3D" active PdZn ensembles [28] which is responsible of modulating the catalysts' selectivity, as suggested by other workers [3,14,18,23]. In addition, patches of surface palladium not properly alloyed with Zn [27] – or just a fraction of pure Pd crystallites- can explain the appearance of CO (S_{CO} < 35%) from MD on those sites, because the eventual concurrency of MSR + RWGS would demand that water conversion were much smaller than X_{CH3OH} which, at least under 573 K, was not observed.

At higher temperature, nonetheless (on Pd/CC–Zn), it is likely that the departure of X_{H2O} respect to X_{CH3OH} (90% vs. 100% at 623 K) and a somewhat smaller S_{CO2} (93% vs. 88% at 573 K vs. 623 K, respectively), could be indicative that the RWGS operates, at least with moderate progress.

Considering now the activity and selectivity performance of the catalysts prepared with the *composite* supports, it was found, in general, that the addition of ZnO to CeO_2 produced noticeable improvements with respect to the Pd/CeO_2 catalysts, regardless of the coprecipitation method that was employed (OC or CC): S_{CO2} was always better for $Pd/ZnO + CeO_2$ vs. Pd/CeO_2, as it was also evident that this outcome was always related to higher water conversion, in every case (Figs. 1 and 2).

In particular, for the smaller Zn/Ce atomic ratios the Pd/OC–ZnCe catalysts were somewhat less selective to CO_2 than their Pd/CC–ZnCe counterparts in the complete range of temperature (and X_{CH3OH}) explored. Likewise, X_{H2O} was always conspicuously smaller than X_{CH3OH} in the first group of catalysts (OC series) than in the second one (CC series). In other words, for Zn/Ce ≤ 1 at/at, the Pd/OC–ZnCe catalysts behaved more similarly to Pd/CeO_2 than the Pd/CC–ZnCe series. Conversely, the latter (and also those with Zn/Ce = 2 at/at regardless of the coprecipitation method used in the oxides syntheses), behaved like Pd/ZnO for temperatures under 548 K, where the MSR prevails. Above said temperature the progressive approach of the measured S_{CO2} to the equilibrium values signaled the impact of thermodynamics, via the progress of the RWGS.

These findings, in combination with our XRD data on the supports structure [11], allow us to infer that by means of the OC synthesis route the ZnO (which was found to have larger crystal sizes and a larger crystallinity degree than in the CC series) achieved less intimacy with Pd than in the Pd/CC–ZnCe *composites* (in which Pd could then be associated to ZnO in larger amount). This fact would be enough to explain why the catalytic

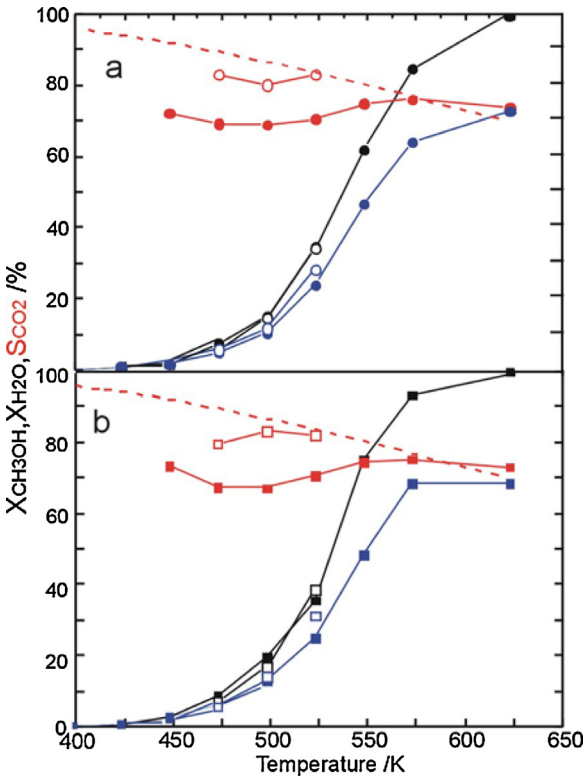

Fig. 4. Percent methanol and water conversions, X_{CH3OH} (black) and X_{H2O} (blue), and percent selectivity to carbon dioxide, S_{CO2} (red), vs. temperature on (a) Pd/IO–ZnCe04 and (b) Pd/IO–ZnCe1. Process conditions and symbols as indicated in Fig. 1. (For interpretation of the references to color in this figure legend, the reader is referred to the web version of this article.)

performance of Pd/OC–ZnCe catalysts was worse, more similar to that of Pd/CeO_2 than their Pd/CC–ZnCe counterparts, in which the proportion of amorphous ZnO was higher [11]. Actually, the best values of S_{CO2} and reactants conversion in the CC series along the whole temperature range was found for the lowest Zn/Ce atomic ratio (Zn/Ce = 0.5 at/at, Fig. 2b).

The two 'conventional' catalysts, Pd/IO–ZnCe04 y Pd/IO–ZnCe1, in which the supports were prepared by impregnating ceria with ZnO, displayed a very similar performance (Fig. 4). At 548 K, for instance, X_{CH3OH} = 75%, X_{H2O} = 66% and S_{CO2} = 75%. These values, in turn, were entirely equivalent to the ones found in the Pd/CC–ZnCe05 catalyst. In other words, both support synthesis methods, CC and IO, allowed to produce better MSR catalysts.

It is timely to point out that just 1 wt% Pd was used to prepare the IO series (seeking to minimize metal loading and assess the impact of such decrease), whereas the supports of the OC and CC series were impregnated with 2 wt% Pd. Yet as the surface-exposed fraction (SEF) of the metal on the catalysts of the IO series doubled the value of the co-precipitated one (20 vs. 10%, see below), the net impact of halving the precious metal loading was, therefore, counterbalanced.

Upon cooling, every ZnO containing catalyst showed better S_{CO2} for comparatively similar X_{CH3OH} (and X_{H2O}) values to those exhibited during the heating steps (see empty symbols in Figs. 1, 2 and 4). A plausible explanation is to posit that under the reaction mixture, and upon heating to 623 K, the surface of the metal crystallites became modified, richer in full 3D active PdZn ensembles, most likely owing to an increase of the Pd–Zn alloying which – in turn- decreased methanol decomposition. This is entirely consistent with recent literature reports [4,28] and our XPS data, as shown below.

To recapitulate matters, Fig. 5 combines CO_2 selectivity vs. methanol conversion for the complete set of catalysts of the OC, CC and IO series. It is readily apparent that both Pd/ZnO catalysts, which were kinetically controlled by the MSR reaction in the entire temperature range, showed the best S_{CO2} values.

The CC *composite* catalysts displayed a seemingly 'anomalous' performance: the higher the ZnO amount employed in their preparation was, the worse the carbon dioxide selectivity became (for isoconversion conditions).

On the OC *composites,* however, the S_{CO2} improved the higher the Zn content was, although vis-á-vis the selectivity to carbon dioxide was always worse than in their CC counterparts. Even though at this point it is not entirely clear why this may be so, it is highly likely that in the *composite* supports prepared by coprecipitating the oxalate salts the ZnO particles, which precipitated with higher crystallinity than in the CC *composites* [11], were partially occluded by the smaller CeO_2 crystals and/or that, due to the higher crystal size and/or crystallization degree of the ZnO particles in the OC preparations – as compared to the ones in the CC counterparts- the surface fraction of ZnO was smaller in the OC series. In both situations, this would lead to both a worse Pd-Zn interaction and a higher impact of the MD (and WGS) vs. the MSR reaction.

Whatever the ultimate reason might be, the Pd/CC-ZnCe05 and Pd/IO-ZnCe04 composite catalysts were the best performing ones. Thus, together with the single oxide Pd/CC–Ce and Pd/CC–Zn catalysts taken as benchmarks, they were chosen as representative materials for further, detailed reaction and spectroscopic studies of our research program. In this regard, the following section gives some catalyst stability data.

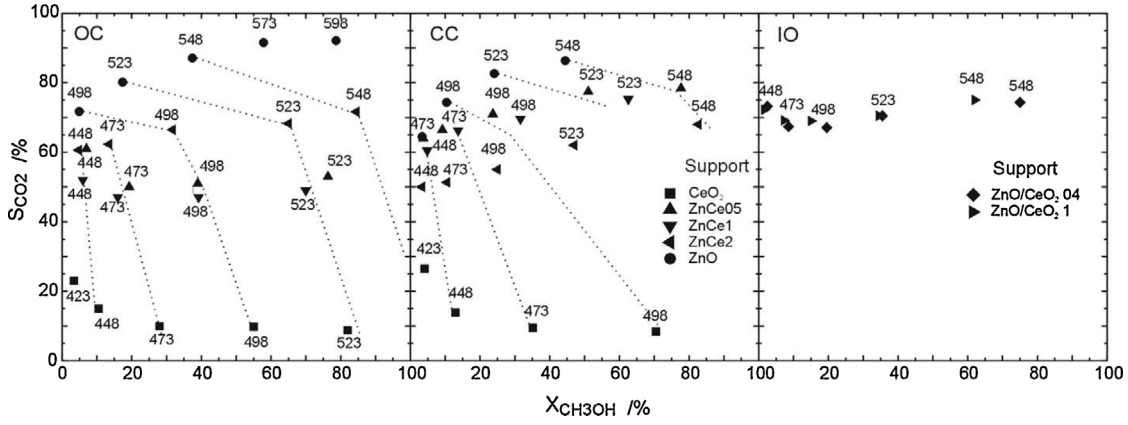

Fig. 5. Evolution of the selectivity to CO_2 as a function of methanol conversion on the Pd catalysts supported on the OC (oxalate co-precipitated), CC (carbonate co-precipitated) and OI (ZnO impregnated onto ceria) support series. The numbers inside the figures indicate the temperature (K) at which each data was taken. Process conditions and symbols as indicated in Fig. 1.

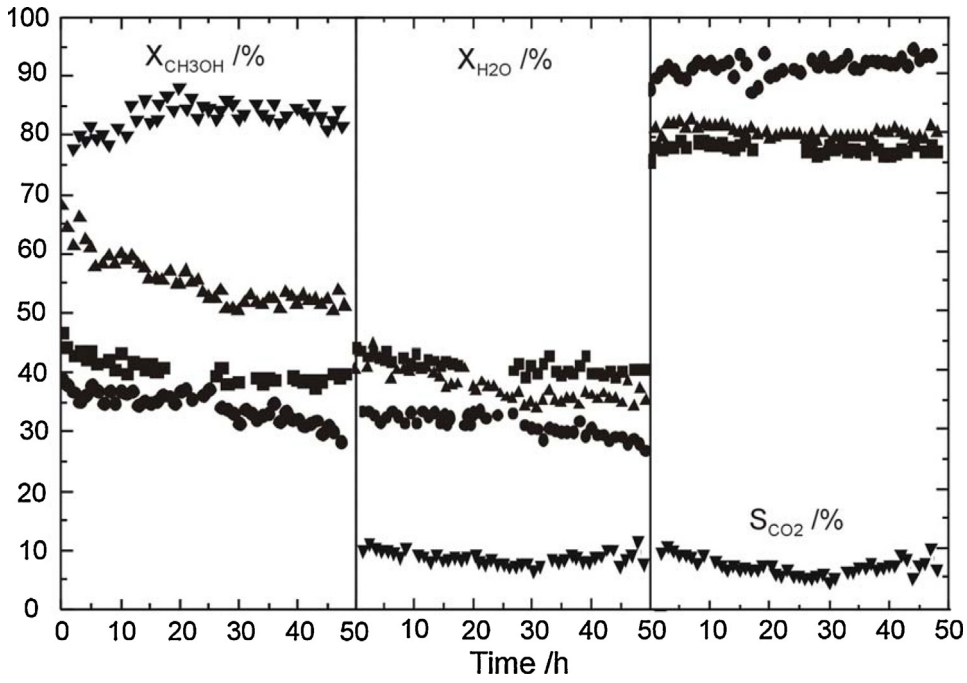

Fig. 6. Stability of selected supported Pd catalysts for the MSR reaction, at 548 K: (▼) Pd/CC–Ce, (●) Pd/CC-Zn, (▲) Pd/CC–ZnCe05 and (■) Pd/IO-ZnCe04. Process conditions: P = 0.1 MPa; $CH_3OH/H_2O/He$ = 6.5/6.5/87 v/v%; GHSV = 64,200 $cm^3\ h^{-1}\ g^{-1}$; W/F^0_{CH3OH} = 240 g h $m^{-3}{}_{CH3OH}$.

3.2. Catalysts stability

Fig. 6 shows the evolution of the reactants conversion (methanol and water) and the selectivity to CO_2 vs. time on stream on the subset of selected catalysts: (2 wt%) Pd/CC–Ce, (2 wt%) Pd/CC–Zn, (2 wt%) Pd/CC–ZnCe05 and (1 wt%) Pd/IO–ZnCe04 (from now on designated with the shorthand labels: Pd/CeO_2, Pd/ZnO, $Pd/ZnO–CeO_2$ and $Pd/ZnO/CeO_2$, respectively) which were evaluated for the MSR reaction at 548 K during 50 h. Since the reactants composition, GHSV and W/F^0_{CH3OH} were close to the ones used in the previous experiments, the initial values of catalytic performances were fairly similar to those exhibited by the materials at such temperature in the activity–selectivity plots shown in Figs. 1 and 2.

For Pd/CeO_2, the conversions of methanol and water, as well as the selectivity to CO_2, remained constant after 18 h on stream: 80, 9 and 8%, respectively. As it was pointed out in the previous section, this catalyst is particularly active for methanol decomposition. It can also be appreciated that the production of CO_2 is closely related to the fraction of H_2O that reacted with CO (the product of MD), via the WGS reaction.

A continuous decrease of methanol and water conversion was observed instead in the case of Pd/ZnO; the catalyst deactivation was steady along the stability test. However, S_{CO2} remained almost constant, at or above 90%.

Both selected *composites*-supported Pd catalysts had a similar behavior at the beginning of the reaction. They exhibited some deactivation during the first 24–28 h, but later stabilized with X_{CH3OH} values of 53 and 40% for $Pd/ZnO–CeO_2$ and $Pd/ZnO/CeO_2$, respectively. Their selectivity to CO_2 remained constant at about 75–80%.

Although the possible causes that may affect the stability of these catalysts will be discussed later, in the context of bimetallic PdZn particles genesis, it is important to remark at this point that it is to be anticipated that their formation under different contexts when comparing Pd/ZnO (namely, on bulk zinc oxide) vs. Pd supported onto the composite oxides may be relevant. Regardless, these results show that the latter catalysts, which exhibited fairly reasonable yields to H_2 and CO_2, were also more stable than the pure Pd/ZnO. Therefore, both $Pd/ZnO–CeO_2$ and $Pd/ZnO/CeO_2$ could be envisaged as interesting alternatives to conduct MSR if, for instance, the process temperature was lowered and the residence times of the reaction mixture (that is, higher W/F) were increased.

Table 2
Surface-exposed fraction (SEF) of Pd in metal crystallites as a function of the reduction temperature.

Catalyst	T_{redn}(K)	SEF (%)		
		CO[a]	H_2[b]	TEM[c]
Pd/SiO_2	623	44	46	52
$Pt/Ce_{0.68}Zr_{0.32}O_2$	473	63	–	65
Pd/CeO_2	423	26	–	–
	623	25	–	n.d.
$Pd/ZnO–CeO_2$	423	13	–	–
	473	12	–	–
	523	11	–	–
	623	8.0	–	45
$Pd/ZnO/CeO_2$	423	26	–	–
	473	25	–	–
	523	20	–	–
	623	21	–	–
Pd/ZnO	298	5.0[e]	–	16[f]
	623	1.2	–	–

n.d.: not detected
[a] Step CO chemisorption under flow, at 298 K (w/CO_2 saturation – see text-).
[b] H_2 chemisorption at 298 K (double isotherm method [31]).
[c] High-angle anular dark-field imaging (STEM-HAADF).
[e] Reduction by hydrogen during 24 h.
[f] Sample calcined at 673 K, unreduced.

3.3. Surface and bulk PdZn alloy formation

3.3.1. Surface-exposed fraction (SEF) of palladium in the metal crystallites

Table 2 shows the SEF values measured by step CO chemisorption (CO-SEF) on the selected catalysts pre-reduced in hydrogen at several temperatures. To validate the technique these CO-SEF

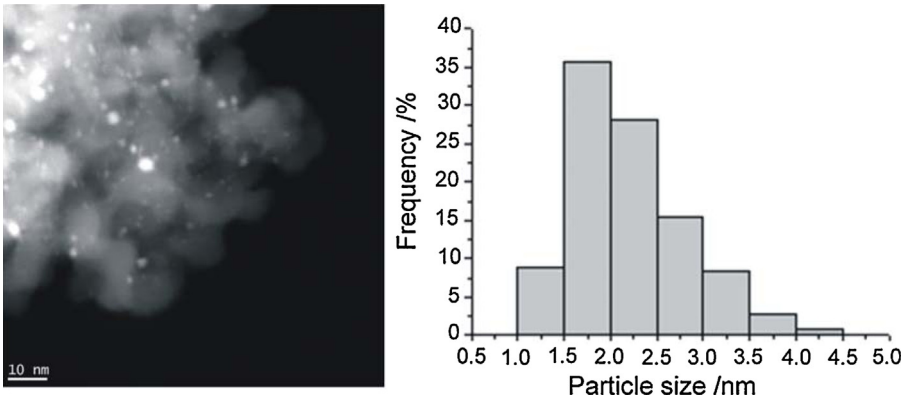

Fig. 7. Z-contrast STEM-HAADF image and particle size distribution histogram of the metal particles of the Pd/SiO_2 catalyst (sample reduced at 673 K).

measurements were compared with SEF estimations made by H_2 chemisorption (H_2-SEF) and/or TEM on well-characterized Pd/SiO_2 and $Pt/Ce_{0.68}Zr_{0.32}O_2$ catalysts. The calculated CO-SEF on Pd/SiO_2 was 44 ± 4%, very similar to the H_2-SEF value, 46% [31]. A further confirmation was made using STEM-HAADF imaging, which neatly showed small Pd crystallites of unimodal size distribution (d_{TEM} = 2.2 ± 0.6 nm) on this catalyst, from which the estimated SEF, using the classic expression for spherical particles (viz., SEF = 1.12/d_{TEM}), was 52% (Fig. 7). Additionally, and after a reduction at relatively low temperature (473 K), the determined CO-SEF value on $Pt/Ce_{0.68}Zn_{0.32}O_2$ benchmark catalyst was close to the one calculated from the TEM measurement (63 vs. 65%, respectively) [29]. Those firm correspondences of the experimental results aimed to determining the SEF, even on reducible supports (but avoiding to generate SMSI effects in the pretreatments,) prompted us to apply the CO-SEF estimation technique to our catalysts as well. In general, as indicated in Table 2, higher pre-reduction temperature led to smaller SEF values, with the exception of Pd/CeO_2 where about 25% was always found. Unfortunately, there was not enough contrast in its STEM-HAADF images to allow any determination of the particle size of the metal particles on this catalyst. Nonetheless, Bernal and coworkers did not observe any change in metal dispersion on (4 wt%) Pt/CeO_2 after reducing treatments at 473 and 623 K (H_2, 2 h), either [32]. In addition, a HRTEM/XRD study on ceria-supported Pd catalysts reported that the onset of nanostructural phenomena related to SMSI effects (such as surface decoration and/or alloy formation with ceria) demanded reduction temperatures at or above 973 K [33]. Therefore, the absence of SMSI effects related to ceria in our case must also be presumed.

The Pd/ZnO catalyst gave extremely low CO-SEF values: 5% after 298 K reduction (24 h) and just 1.2% after reducing at 623 K. Even though this support had a modest surface area, for which low metal dispersion was anticipated, it is also likely that these low SEF values could be ascribed to either large crystallite sizes and/or the formation of a Pd–Zn surface alloy, which could then (at least partially) decrease the amount of CO chemisorbed by the surface of the metal particle, as it has been reported that at room temperature CO chemisorbs much less on (unsupported) tetragonal $PdZn\beta_1$ nanoalloys than on fcc $PdZn\alpha$ or bulk Pd [27]. Since the heat of adsorption of CO on Pd decreases upon PdZn alloy formation, it is also possible that a certain fraction of surface Pd would not be detected (even under a constant, superimposed CO pressure). Then, these CO-SEF determined values would be minimum ones but, again, this would be a proof of the surface PdZn alloying.

Fig. 8 shows a Z contrast image of the Pd/ZnO catalyst, after calcining the material at 673 K. The mean particle size of the metal particles (d_{TEM}) was 7.7 ± 3.1 nm, that is, with a wide size distribution. Using the average value, the calculated metal dispersion (again, considering spherical particles) was 15.7%.

The image contrast of the reduced samples was insufficient to allow particle size measurements but, nonetheless, the CO-SEF values would be considerably lower than the ones estimated by electron microscopy if a Pd–Zn alloy was (at least superficially) formed, even after RT reduction for 24 h (Table 2).

The surface-exposed metal fraction of the palladium catalyst supported on the coprecipitated $ZnO–CeO_2$ *composite* was 13% after reduction at 423 K. This value progressively decreased by aprox. 38% at higher reduction temperatures. On the catalyst prepared by supporting Pd on ZnO-impregnated ceria, $Pd/ZnO/CeO_2$, the CO-SEF after reduction at 423 K was about twice (26%) and, likewise,

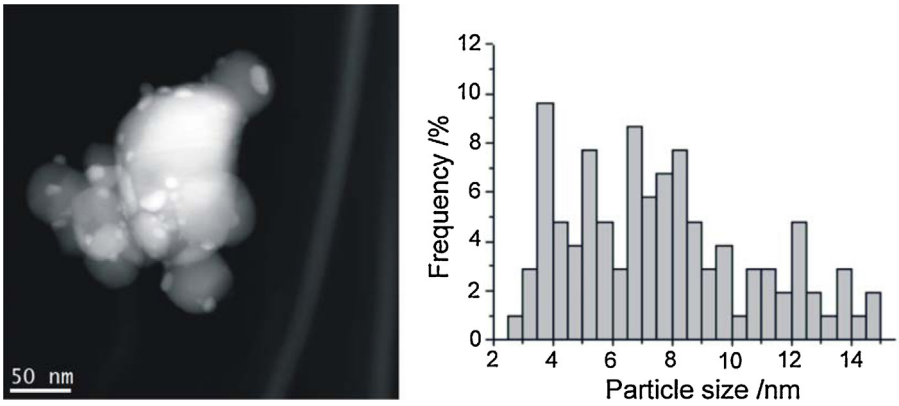

Fig. 8. Z-contrast STEM-HAADF image and particle size distribution histogram of the (bi)metallic particles of the Pd/ZnO catalyst (sample calcined at 673 K).

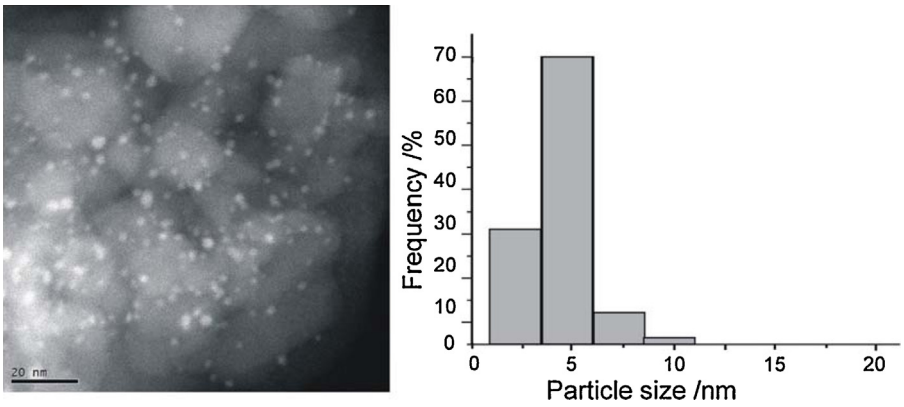

Fig. 9. Z-contrast STEM-HAADF image and particle size distribution histogram of the (bi)metallic particles of the Pd/ZnO–CeO_2 catalyst (sample reduced at 623 K).

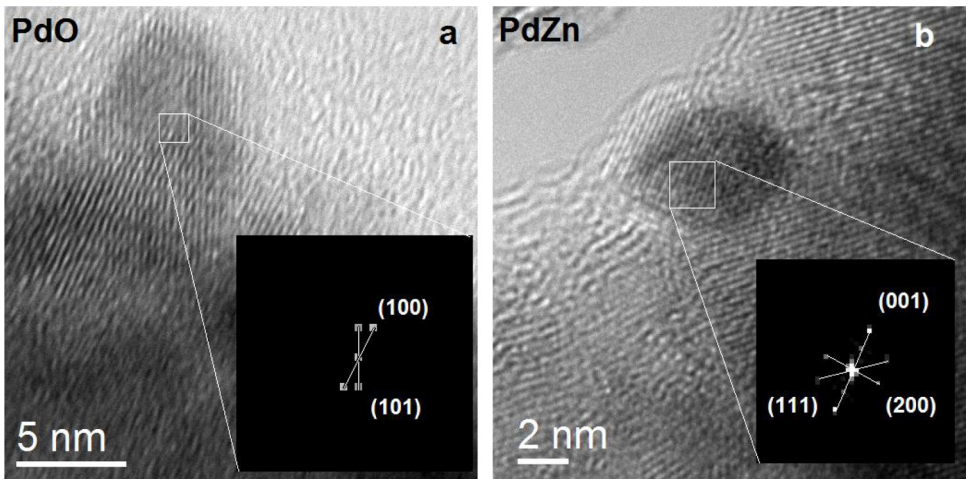

Fig.10. Z-contrast STEM-HAADF image and particle size distribution histogram of the (bi)metallic particles of the Pd/ZnO–CeO_2 catalyst. Samples were pre-reduced at 423 K (a) and 623 K (b), respectively.

the exposed metal fraction became smaller (roughly 20%) with higher reduction temperature (Table 2). Only the first material exhibited a Z contrast good enough to allow the size estimation of the (bi)metallic particles. Fig. 9 shows a dark-field image, together with the corresponding histogram, of the Pd/ZnO–CeO_2 catalyst after reduction at 623 K and passivation at RT. An unimodal distribution, with a mean $d_{TEM} = 2.5 \pm 1.1$ nm was found. This implies a microscopy-calculated SEF equal to 45%, which is five-fold higher than the CO-SEF estimation (Table 2). This huge discrepancy can only be explained by considering that a PdZn surface alloy was formed. To probe this hypothesis, detailed HRTEM measurements were made on the samples reduced in hydrogen at 423 and 623 K, and then air passivated (Fig. 10a and b). The analyses of plane spacing of the metal crystallites of the Pd/ZnO–CeO_2 catalyst reduced at 423 K indicated the presence of both PdO ($d = 3.03$ and 2.63 Å, from the (1 0 0) resp. (1 0 1) planes, JCPDS 85-0624) and the PdZn alloy ($d = 3.32$, 2.19 and 2.05 Å, corresponding to the (0 0 1), (1 1 1) and (2 0 0) diffracting planes, respectively (JCPDS 06-0620). Only the crystal planes pertaining to PdZn alloys (but none from PdO) were observed after the 623 K reduction.

All this set of results clearly indicates that even upon reducing at RT a portion of the noble metal is already (surface) alloyed with zinc and, also, that these bulk alloys were not broken or destabilized upon air exposure.

3.3.2. XPS analyses

Complementary studies aimed to confirming the formation of PdZn alloys on the Pd/ZnO, Pd/ZnO–CeO_2 and Pd/ZnO/CeO_2 catalysts were made. As mentioned above, prior to the XPS measurements each sample was treated in situ in the attached pre-treatment chamber under oxidative and reductive conditions: (1) O_2-623, (2) H_2-423 and (3) H_2-623.

The XPS spectra of Ce 3d core electron levels for both the Pd/CeO_2 and the mixed oxides catalysts were quite similar, showing only Ce^{4+} features in the oxidized samples and progressive reduction of ceria after each H_2 reduction, with the classical, convoluted Ce^{4+} and Ce^{3+} signals [34,35]. The u''' peak, assigned to the highest energy of the Ce 3d multiplet transitions [34], kept constant both peak position and broadening, which confirms that charging effect was adequately compensated. Additionally, the XP reference spectra of C 1s and those of O 1s displayed the expected formation of some carbonate species, which is typical for cerium and zinc oxide (see Figs. S2 and S3 in Supplementary information).

Fig. 11 shows the Pd 3d doublet spectra (Pd $3d_{3/2}$ and $3d_{5/2}$) for the selected samples. In what follows the analyses will focus only on the Pd $3d_{5/2}$ signal, as this peak exhibits better features (viz., characteristic differences in binding energy – BE- and shape), to discriminate the different chemical states of Pd.

The calcined samples showed just a single signal (BE = 336.9 eV), which is typical of Pd^{2+} species [13,17,30,36,37]. After H_2 reduction at 423 K, the Pd 3d transition shifted to much lower BE values. For Pd/CeO_2 the peak maximum was observed at 335.3 eV, and it can be unambiguously assigned to metallic Pd (i.e., Pd^0), in good agreement with literature data [36,38]. After reduction at 623 K, this peak remained in the same position and with the same FWHM. Instead, for Pd/ZnO, Pd/ZnO–CeO_2 and Pd/ZnO/CeO_2 the Pd $3d_{5/2}$

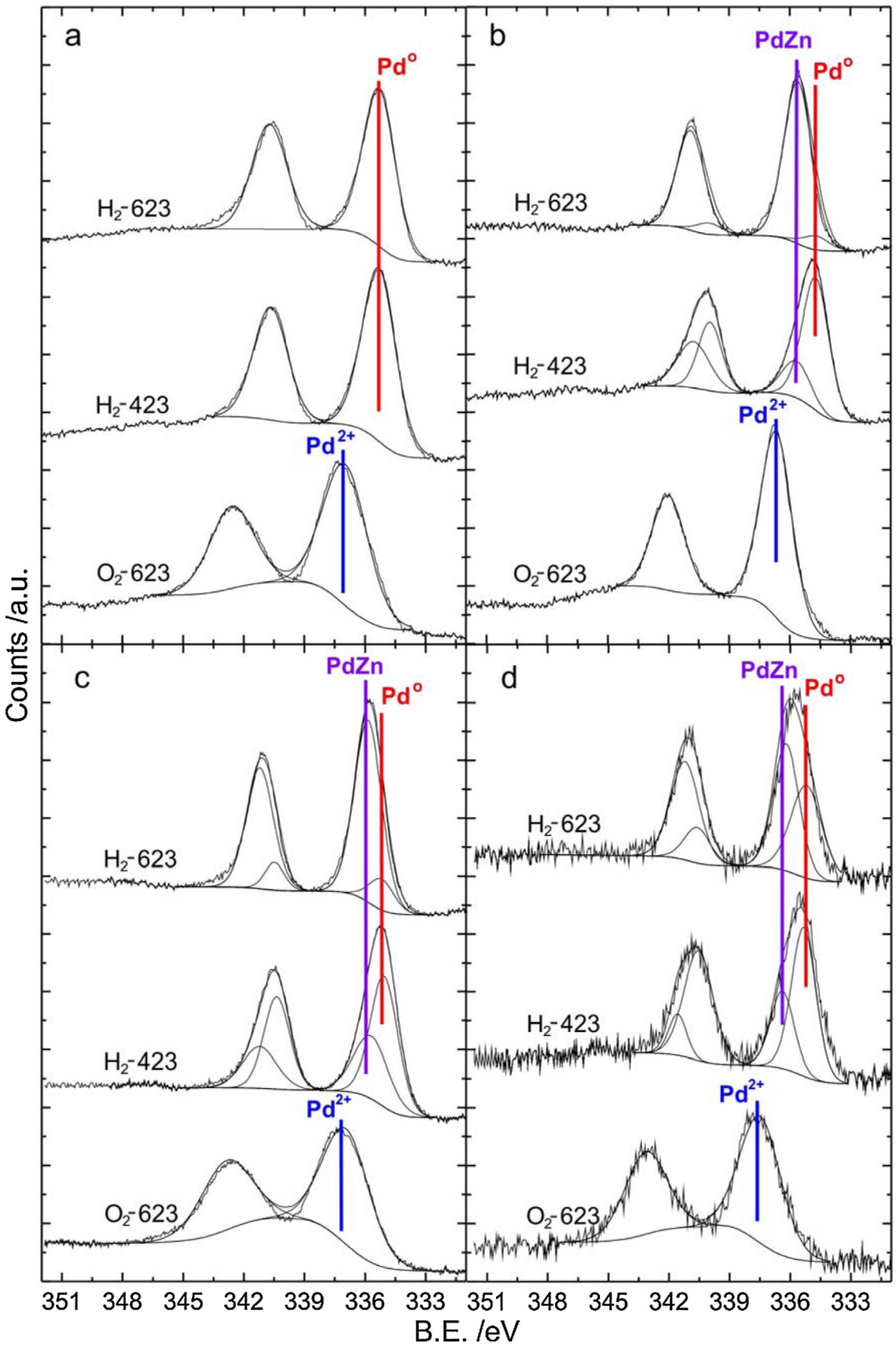

Fig. 11. XPS spectra of the Pd 3d region of the supported Pd catalysts subjected to calcination (O_2, 623 K) and hydrogen reduction (H_2, 423 and 623 K) pretreatments: (a) Pd/CeO_2, (b) Pd/ZnO, (c) $Pd/ZnO–CeO_2$ (Pd/CC–ZnCe05) and (d) $Pd/ZnO/CeO_2$ (Pd/IO–ZnCe04).

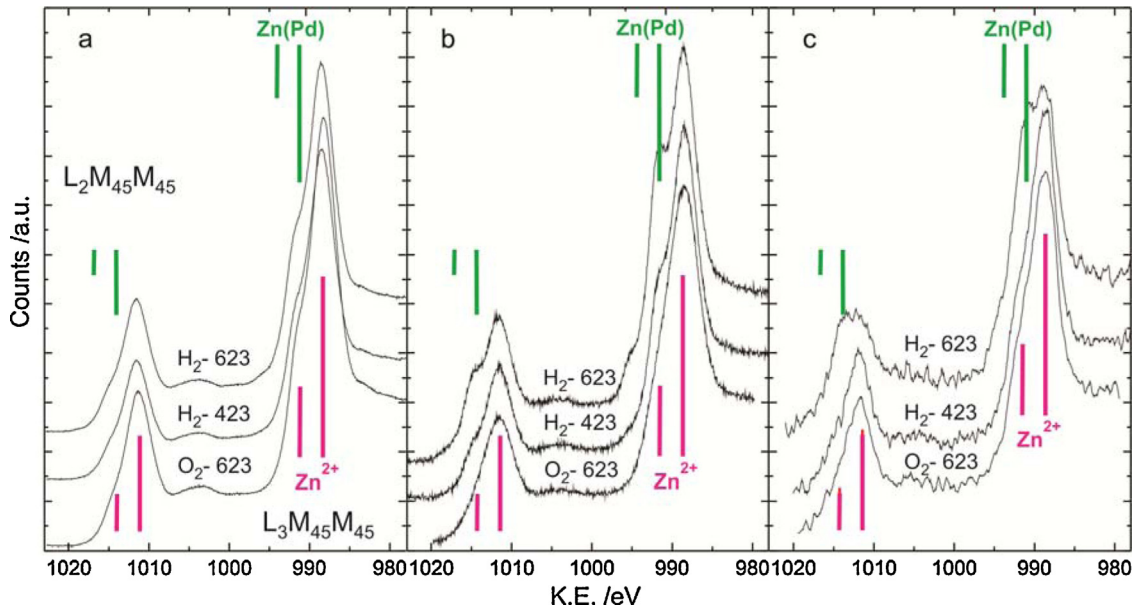

Fig. 12. XPS spectra of the Zn LMM Auger signals for the (a) Pd/ZnO, (b) Pd/ZnO–CeO_2 and (c) Pd/ZnO/CeO_2 catalysts subjected to calcination (O_2, 623 K) and hydrogen reduction (H_2, 423 and 623 K) pretreatments.

peak maxima first shifted to lower BEs after the H_2-423 treatment, but said maxima became located at higher BEs (and with narrower FWHMs) after the H_2-623 treatment, thus showing that the signal could not be properly fitted to a single component and strongly implying that the Pd species on the 423 K reduced catalyst were already in multi-chemical states. XPS studies of Pd–Zn interaction have confirmed that PdZn alloys formation leads to an increase in the BE of Pd metal. The chemical shift reported in different studies [13,15,36,37,39] varies from +0.6 to +1.0 eV. The deconvoluted Pd 3d signals in Fig. 11 show that palladium is already partially alloyed after the H_2-423 treatment in all the Zn-containing supports, and is mostly alloyed after the H_2-623 reduction treatment (see the deconvoluted peak at approximately 335.8 eV).

The spectra of the Zn $2p_{3/2}$ peak taken after calcining showed much broader bands for the Pd/ZnO–CeO_2 and Pd/ZnO/CeO_2 catalysts than for Pd/ZnO, indicating a certain degree of interaction between the oxide domains (see Fig. S4 in Supplementary information). After the H_2 treatments a small, progressive shift to lower binding energies (0.2–0.3 eV) could be appreciated. As it has been reported by several authors [13,37,40] the alloying of Pd and Zn increases the binding energy of the core and valence levels of Pd but reduces the binding energy of the core and valence levels of Zn, which is consistent with our results.

In agreement with these findings, spectra of the Zn Auger LMM region were recorded to discriminate between metallic and oxidized Zn species, during the entire reductive treatment. The Auger spectrum of zinc, and those of other elements such as Cu, Ga and Ge, is the result of several electronic transitions [41,42]. For Zn, the most intense Auger processes, $L_3M_{45}M_{45}$ and $L_2M_{45}M_{45}$, have been both characterized by two final states that can explain approximately 90% of each Auger process, being the L_3 transition roughly twice more intense than the L_2 one and the ratio between the intensities originated by those final states ~2.6 [42]. Our results clearly show that in all the zinc-containing catalysts after the oxidizing treatment (O_2-623, that is, where only ZnO is present on the samples) both bands, located at 988 and 1011 eV, have a shoulder at higher energy values (see Fig. 12, in which both final states are depicted by purple vertical bars), in agreement with Schön's results on pure ZnO [41].

Moreover, these two processes (L_3 and L_2) are qualitatively almost identical for either Zn^{2+} or Zn^0, but they are energetically different: the Auger peaks for Zn^0 are shifted to higher KE values with respect to those of Zn^{2+} (between 2 and 3 eV) [41]. As a consequence, after further reducing treatment (and at higher temperatures) of our Pd/ZnO–CeO_2 and Pd/ZnO/CeO_2 selected catalysts, three overlapped peaks became neatly discerned in the XPS spectra, at 991, 995 and 1014 eV (Fig. 12), which are assigned to metallic Zn in the intermetallic PdZn in accordance with other works [17,30,41]. These last features were less clear for the Pd/ZnO catalyst (Fig 12a), as expected, because there the amount of ZnO overwhelms that of Zn^0.

4. Discussion

Our methanol reforming studies at atmospheric pressure using a diluted, stoichiometric methanol/water mixture showed that only methanol decomposition (MD) occurred on Pd/SiO_2, throughout the entire X_{CH3OH} range, thus indicating that whenever the Pd particles are supported onto an inert (or non-active support) the only product is CO. For that catalyst water behaves, then, just as an inert component of the reaction mixture. However, the catalysts prepared using a water-interacting support such as CeO_2 were not only more active than Pd/SiO_2 but also substantially less selective to CO due to the impact of the WGS reaction, which is entirely consistent with the results of other works [43–45]. Gorte and Zhao [46] compared the WGS reaction rate using CeO_2, Pd/CeO_2 and Pd/Al_2O_3 under differential conversion conditions. At 500 K, for instance, they found that the reaction rate on Pd/CeO_2 was 50-fold higher than on Pd/Al_2O_3 and/or on pure CeO_2. So, the authors emphasized the need of the precious metal and the ceria for the achievement of high WGS activity. Along these lines, Bunluesin et al. [47] compared the performance in the WGS reaction of Pd, Rh and Pt supported on CeO_2, showing that the three metals were equally effective. Both studies concluded that the WGS mechanism proceeded jointly on the metallic particles and the ceria support.

The Pd/ZnO catalysts using either support preparation method (OC or CC) were far less active but much more selective toward

the desired MSR reaction, which is expected and congruent with several authors' findings. However, the precise nature of this exceptional catalytic behavior is yet to be firmly established since, to the best of our knowledge, an in-depth surface analysis under real reaction conditions (*operando*) has not been published yet.

Datye and co-workers have systematically studied the performance of Pd/ZnO and Pd–ZnO/Al_2O_3 catalysts for the MSR, WGS and RWGS reactions, seeking to correlate the experimental values of activity and selectivity with the presence (or absence) of a PdZn alloy as the key or determining factor of the catalysts' performance [7,20–23,48]. They characterized the (bi)metallic PdZn particles by means of bulk techniques (e.g., XRD and STEM), both of which call for crystallinity of the observables to draw any inference or conclusion, though. Their MSR experiences on (7.4 wt%) Pd/ZnO (molar ratio $H_2O/CH_3OH = 1$, $P = 1$ atm, $T = 523$ K, [23]) indicated that low CO selectivity was associated with the presence of larger PdZn particles (>2 nm). For instance, at isoconversion ($X_{CH3OH} = 67$ %) small diameter PdZn crystallites (1.5 nm) gave $S_{CO} = 19$ %, whereas 2.2 nm PdZn particles gave $S_{CO} = 7$%. They also pointed out that the presence of non-alloyed Pd together with the PdZn particles also gave a low CO selectivity ($S_{CO} = 5$%), quite comparable with that of a sample in which all the precious metal was alloyed ($S_{CO} = 4$%) [23]. The combined analyses allowed the authors to postulate that the MSR reaction proceeded at the Pd–ZnO interface, minimizing the impact of the presence – or formation- of an alloy as the only, determining factor of activity and selectivity in the steam reforming reaction on those catalysts.

However, in a contemporary work Wang and co-workers [19] observed that a higher pre-reduction temperature of their (10 wt%) Pd/ZnO catalysts led to PdZn crystallites of ~11.4 nm, with better selectivity to CO_2 in the MSR reaction than the materials that were pre-reduced at a lower temperature (523 K, 4.5 nm PdZn particles). Soon afterwards, both groups jointly studied the RWGS reaction on these Pd/ZnO catalysts [21], observing that the CO_2 conversion decreased on larger PdZn bimetallic particles. These results for the RWGS reaction were predicted by theoretical calculations, which suggested that the production of CO is favored on surface defects of the PdZn alloy [49]. Hence, it is to be expected that larger particles would have less defects (borders, steps, corners, among others) and that, therefore, would not favor the formation of CO in the RWGS.

On the other hand, in their combined study of the MSR, WGS, and RWGS reactions on Pd–ZnO/Al_2O_3 catalysts (Pd/Zn atomic ratio = 0.5), these groups reported similar values of the MSR and WGS pseudo-first order kinetic rate constants, about 20-fold higher than that of the RWGS reaction. They indicated that this last reaction (onto the PdZn alloy) could only partially explain the genesis of CO production, posing that CO was also generated by methanol decomposition on metallic Pd sites [20].

In our experiments on Pd/ZnO it could also be appreciated that the RWGS reaction was kinetically controlled at lower temperature (note that the CO_2 molar fraction was above the thermodynamic equilibrium value, see Figs. 1 and 2e) but, nevertheless, discernible at higher temperature (by the progressive convergence of the exit composition from the reactor toward equilibrium values).

It is convenient to emphasize that in the abovementioned work by Datye et al. [20], neither methanol conversion (60–65%) nor CO selectivity (7–5%) varied significantly whenever the methanol/water molar ratio was changed, thus indicating that the impact of this factor in the kinetic rate expressions was negligible under their working conditions ($p_{CH3OH} = 0.21$ MPa, $T = 493$ K). In fact, that was the basis for selecting a single (equimolar) feed condition in our experimental program.

Datye and coworkers also evaluated the effect of ZnO morphology on MSR using powder Pd/ZnO catalysts [48]. For same-size of PdZn crystallites (7.5–10 nm), zinc oxides with different morphology (i.e., exposing different surface planes) had different catalytic performance, which prompted the authors to consider that ZnO functioned, not only as support and source/partner for the PdZn alloy but, also, as an active participant in intermediate steps in the MSR reaction.

Bera and Vohs [25] performed surface science studies on model Pd/ZnO(0001), catalysts, suggesting that Zn sites (located both at the Pd/ZnO interface and onto the Pd/Zn alloy) could act as active, oxygen donor sites reacting with the CO chemisorbed on the metal, thus producing CO_2. However, it must be pointed out that it is highly unlikely that that was the reaction pathway for CO_2 production under MSR conditions on Pd/ZnO because under their operating conditions the S_{CO2} would have been limited to significantly lower values than the ones that were experimentally observed by them.

We believe it more likely that (like in our catalysts) the RWGS was acting as a modulator of the selectivity to CO_2 *a posteriori* of the MSR, as it also emerges from Datye and coworkers analyses [7,20–23,25,48] in regards several catalytic materials based on Pd/ZnO.

At this point, it is advisable to recall that Haghofer et al. [50], looking for the origin of the CO generated in their MSR work with Pd/Ga_2O_3 catalysts (known to form Pd–Ga alloys) studied the MD and RWGS reactions (under differential conditions, and using the expected CO_2:H_2 = 1:3 product ratio). For these conditions, they found that the activity for the RWGS reaction was negligible, which would not be able to explain the large amount of CO that was produced under MSR reaction conditions at high temperature (< 10%). So, the authors proposed that MD was the most likely source of CO under reaction conditions, suggesting the existence of a dynamic equilibrium between the formation (via hydrogenation) of a Pd_2Ga intermetallic, selective to MSR, and its decomposition by CO (due to surface restructuring of the Pd particles). As a consequence, they concluded, carbon monoxide production via MD onto metallic Pd patches cannot be entirely prevented, due to the detrimental impact of CO on the selective Pd_2Ga intermetallic compound.

As it was shown recently by us, CO chemisorption on Pd/ZnO catalysts also restructures the PdZn particles, generating di-coordinated and hollow, CO_{B+H}, chemisorption sites [51]. This calls for a detailed *operando* spectroscopic study of the catalysts under MSR conditions, to gain more insight on the possible impact of a progressive, *onstream* destruction of the surface PdZn domains (that are formed/generated in the reduction pretreatment and which allow preventing the detrimental presence of Pd *ensembles* on the surface of the bimetallic PdZn crystallites) on the reaction pathway. This study is presently under way.

In regards the catalysts prepared with the nanocomposite supports it is encouraging that, even though they were less active and selective to the MSR reaction than the Pd/ZnO catalysts, they were all more stable. The CC-series catalysts, prepared by coprecipitating ceria and zinc carbonates, were more selective to CO_2 than the OC materials, synthesized from the oxalates. The former were somewhat closer to Pd/ZnO, where the MSR, rather than the MD, reaction prevails. Again, the ZnO impregnated ceria preparations (IO series) had very similar performance (namely, their S_{CO2} and X_{CH3OH} patterns) to the CC-series. Moreover, even though the palladium loading was just 1 wt% (instead of 2 wt%), they were equally active and selective.

The outstanding issues, then, are not only the need to modify the geometrical/electronic environments of Pd, as the alloying with Zn seems to accomplish (as shown by XPS and TEM), but also the need to provide surface sites onto which methanol can chemisorb and where the intermediates of the MSR reaction are able to react, in conjunction with the (bi)metallic particles. Under these premises, the best performing catalysts would be highly active, selective and stable materials for which: (i) ZnO were highly dispersed on the

surface and – therefore- where the chances of Pd–Zn intimacy prior to pre-reduction were higher (so as to grant the formation of full 3D active PdZn ensembles [28] in as much as possible), and (ii) the catalyst surface area were at least several fold higher than that of pure ZnO.

We believe that our nanocomposite Pd/ZnO–CeO_2 and Pd/ZnO/CeO_2 preparations represent an encouraging step in these directions, in agreement with recent MSR studies by Iwasa and Takezawa [5,30,41,52] and Zhang and Farrauto [3], where CeO_2 supported palladium catalysts modified with zinc were used. Both research groups concurred in that the presence of ceria greatly improved catalyst stability.

In the stability tests shown in Fig. 5, after the incorporation of ZnO to the ceria, either via coprecipitation with or via impregnation to the ceria, the conversion to methanol was steady ($X_{CH3OH} \sim 50$ %), with CO_2 selectivity of about 80% in both cases, thus justifying the designation of CeO_2 as an 'active dispersant of ZnO'. Nonetheless, although the overall performance of these catalysts was far better than that of Pd/ZnO alone (notably in regards stability), their selectivity was still less than desirable.

The deactivation process on Pd/ZnO was steady: after 48 h on stream about 20% of the initial activity was lost. For these catalytic systems, the main causes for deactivation are attributed to loss or occlusion of active sites. Under MSR conditions it has been reported that the PdZn alloy can become occluded by formation of zinc hydroxycarbonate [53] or carbon [20,54], or segregation of metallic Pd and ZnO from the bimetallic particles [14].

Zhang and Farrauto, on the other hand, identified coking as the main culprit for their Pd/Zn/ceria catalysts deactivation [3]. Nonetheless, because their catalysts were synthesized by impregnating powdered ceria with Zn and Pd nitrates, said catalysts were – actually- much less active than ours, which led them to operate at 400 °C instead of just 250 °C as is our case, for the same conversion and about same space velocity. In this way, they took advantage that there are fuel cell processes that require 400 °C operation, so that the CO produced and rejected from the hydrogen permeable membrane as a component of tail gas can then be combusted to provide the endothermic heat of reaction for reforming. After 800 h onstream using a CH_3OH/H_2O stoichiometric mixture at 400 °C and GHSV = 68,000 h^{-1} they measured by XPS about 1% percent increase in the atomic percent of surface carbon (7.1 in the aged catalyst vs. an initial value of 6.1 in the fresh sample) which, roughly speaking, represents about 1 μmol carbon per gram of catalyst or – in other words- about 0.06% of the moles of methanol that were fed to the reactor.

The activation energy for coking is high, though. By halving the coking reaction rate every 10 °C (using the classic rule-of-thumb approach), had we conducted stability studies for 800 h under our experimental conditions (250 °C instead of 400 °C) our catalysts would have accumulated $1/2^{15} = 3.05 \times 10^{-5}$ less surface carbon than those of Farrauto's team, which is indeed a negligible amount, not measurable by XPS nor TPO-MS. We are in no position to predict what the long-term stability of our catalysts will be (hydrothermal processes do occur...) but certainly we surmise that deactivation by coking will not represent the main cause for said (eventual) deactivation.

Our strategy of coprecipitating (or depositing) ZnO with (or on) an active support of intermediate surface area such as ceria, with its well-known reducibility and/or its capability for producing oxygen vacancies [55,56], resulted an efficient tool for the understanding of the underlying catalytic chemistry of these ternary catalysts.

Our experimental results indicate that methanol participates together with the composite support for the steam reforming reaction to proceed efficiently. Indeed, methanol decomposition data (detailed in the Supplementary information section) neatly indicate that the presence of ZnO, either pure or impregnated/coprecipitated with ceria, is essential. That is, it is not just the presence of a PdZn alloy what determined the high activity and CO_2 selectivity that was observed, at least for the process conditions used in this work. While the PdZn alloying seems to play the key role of preventing MD, and the desired (conventional) role of metal crystallites is to release H_2 via inverse spillover, these results also suggest that the main MSR reaction is taking place mostly on an oxidized surface. In particular, the presence of well-dispersed ZnO domains on the support surface and/or as patches onto the PdZn bimetallic crystallites under MSR reaction condition, seems to be crucial for obtaining high turnover frequencies. Nonetheless, other authors have concluded that just the right PdZn alloy (namely, tetragonal PdZnβ_1) suffices to grant high S_{CO2} and high TOF values [26], albeit under MSR conditions oxidized Zn species seem to be present in their pre-reduced bimetallic particles as was suggested by Lorenz et al. [28] based on their relevant XPS spectra, probably because those alloy powders were again exposed to water.

5. Conclusions

Although disperse palladium (1–4 nm particle size) onto an inert support such as silica is only able to decompose methanol in the MSR reaction, over the surface of pure ceria (approximately 4 nm average metallic particle size, or SEF = 25%) it is also capable to activate the (reverse) water gas shift reaction, which suggests that CeO_2 can effectively modulate the selectivity to CO_2 under methanol steam reforming conditions.

On the binary oxide supports, ZnO–CeO_2 or ZnO/CeO_2, palladium showed a catalytic behavior closer to Pd/ZnO, in which it is the steam reforming reaction what selectively takes place, but a detrimental production of CO occurs at high temperature, which can be explained by the concurrent onset of the RWGS reaction.

The incorporation of Zn in the supports' formulation is clearly responsible for the occurrence of a palladium–zinc alloy (Pd:Zn = 1:1). After reduction in H_2 at 623 K, not only the bulk PdZn intermetallic was detected by TEM, which was resistant to oxidation at atmospheric conditions according to these results, but also the bimetallic PdZn surface formation was apparent by comparing the TEM data with the surface exposed fraction of palladium as determined by step CO chemisorption (under CO_2 exposure to avoid CO spillover or adsorption on the support). Since Pd/ZnO catalyst worked under kinetic (rather than thermodynamic) control almost in the entire temperature range tested, it seems plausible, then, that the formation of a bimetallic surface is a *sine qua non* condition to prevent – at least partially- the deleterious production of CO. Nonetheless, as rightly pointed out by one of our reviewers, some MSR designers purposely operate at >573 K (and use Pd membranes) where the tail gas contains some CO which is combusted to provide heat for the endothermic MSR reaction, thus allowing a more efficient, energy integrated process [3,9,10].

A better understanding of the catalysts' pretreatment for PdZn stabilization on these ceria-based supports, together with lower temperature of reaction and higher W/F^0_{CH3OH}, can be envisaged as possible alternatives to develop a technological process aimed to obtaining a CO_2 selectivity higher than 90% for full methanol conversion, operating even under the WGS thermodynamic equilibrium regime. Otherwise, necessarily, the employment of temperatures higher than 450 K to allow for acceptable catalytic activity levels, would impose an impossible constraint in terms of selectivity.

Acknowledgements

The authors acknowledge financial support for this work from ANPCyT of Argentina (PICT 2012 1280, PME 2006 311 and PME

2003 8) and Universidad Nacional del Litoral (CAID 2011 PI 50120110100311). The authors kindly thank Drs. J.J. Delgado and S. Bernal for supplying the Pt/Ce0.68Zr0.32O2 sample, and Dr. R. Zanella for the discussion and interpretation of the TEM images. C.B. thanks CONICET for the fellowship received to do this work.

Appendix A. Supplementary data

Supplementary data associated with this article can be found, in the online version, at http://dx.doi.org/10.1016/j.apcatb.2015.05.030

References

[1] R. Palo, R.A. Dagle, J.D. Holladay, Chem. Rev. 107 (2007) 3992–4021.
[2] S. Sá, H. Silva, L. Brandao, J.M. Sousa, A. Mendes, Appl. Catal. B: Environ. 99 (2010) 43–57.
[3] Q. Zhang, R.J. Farrauto, Appl. Catal. A: Gen. 395 (2011) 64–70.
[4] M. Armbrüster, M. Behrens, K. Föttinger, M. Friedrich, E. Gaudry, S.K. Matam, H.R. Sharma, Catal. Rev. -Sci. Eng. 55 (3) (2013) 289–367.
[5] N. Iwasa, T. Mayanagi, W. Nomura, M. Arai, N. Takezawa, Appl. Catal. A: Gen. 248 (2003) 153–160.
[6] P. Pfeifer, A. Kölbl, K. Schubert, Catal. Today 110(1-2)(2005) 76-85.
[7] T. Conant, A.M. Karim, V. Lebarbier, Y. Wang, F. Girgsdies, R. Schlögl, A. Datye, J. Catal. 257 (2008) 64–70.
[8] F.J. Echave, O. Sanz, M. Montes, Catal. Today 213 (2013) 145–154.
[9] O.M. Ilinich, Y. Liu, C.R. Castellano, G.S. Koermer, A. Moini, R.J. Farrauto, Platinum Met. Rev. 52 (2008) 134–143.
[10] C.R., Castellano, Y., Liu, A., Moini, G.S., Koermer, R.J., Farrauto, US Patent 7,569,511B1 (August 4, 2009).
[11] C.E. Barrios, M.A. Baltanás, R. Bolmaro, A.L. Bonivardi, Powder Technol. 267 (2014) 180–192.
[12] D.L. Chiavassa, J. Barrandeguy, A.L. Bonivardi, M.A. Baltanás, Catal. Today 133–135 (2008) 780–786.
[13] J.L. Rodríguez, J. Phys. Chem. 98 (1994) 5758–5764.
[14] K. Föttinger, J.A. Van Bokhoven, M. Nachtegaal, G. Rupprechter, J. Phys. Chem. Lett. 2 (2011) 428–433.
[15] C. Rameshan, C. Weilach, W. Stadlmayr, S. Penner, H. Lorenz, M. Hävecker, R. Blume, T. Rocha, D. Teschner, A. Knop-Gericke, R. Schlögl, D. Zemlyanov, N. Memmel, G. Rupprechter, B. Klötzer, J. Catal. 276 (2010) 101–113.
[16] C. Rameshan, W. Stadlmayr, C. Weilach, S. Penner, H. Lorenz, M. Hävecker, R. Blume, T. Rocha, D. Teschner, A. Knop-Gericke, R. Schlögl, D. Zemlyanov, N. Memmel, G. Rupprechter, B. Klötzer, Angew. Chem. Int. Ed. 49 (2010) 3224–3227.
[17] M. Friedrich, D. Teschner, A. Knop-Gericke, M. Armbrüster, J. Catal. 285 (2012) 41–47.
[18] Y.H. Chin, Y. Wang, R.A. Dagle, X.S. Li, Fuel Process Technol. 83 (2003) 193–201.
[19] R.A. Dagle, Y.H. Chin, Y. Wang, Top. Catal. 46 (2007) 358–362.
[20] R.A. Dagle, A. Platon, D.R. Palo, A.K. Datye, J.M. Vohs, Y. Wang, App. Catal. A: Gen. 342 (2008) 63–68.
[21] V. Lebarbier, R.A. Dagle, A. Datye, Y. Wang, Appl. Catal. A: Gen. 379 (2010) 3–6.
[22] V. Lebarbier, R.A. Dagle, T. Conant, J.M. Vohs, A. Datye, Y. Wang, Catal. Lett. 122 (2008) 223–227.
[23] A. Karim, T. Conant, A. Datye, J. Catal. 243 (2006) 420–427.
[24] E. Jeroro, J.M. Vohs, J. Am. Chem. Soc. 130 (2008) 10199–10207.
[25] P. Bera, J.M. Vohs, J. Phys. Chem. C 111 (2007) 7049–7057.
[26] B. Halevi, E.J. Peterson, A. DeLaRiva, E. Jeroro, V.M. Lebarbier, Y. Wang, J.M. Vohs, B. Kiefer, E. Kunkes, M. Havecker, M. Behrens, R. Schlögl, Abhaya K. Datye, J. Phys. Chem. C 114 (2010) 17181–17190.
[27] B. Halevi, E.J. Peterson, A. Roy, A. DeLariva, E. Jeroro, F. Gao, Y. Wang, J.M. Vohs, B. Kiefer, E. Kunkes, M. Hävecker, M. Behrens, R. Schlögl, A.K. Datye, J. Catal. 291 (2012) 44–54.
[28] H. Lorenz, C. Rameshan, T. Bielz, N. Memmel, W. Stadlmayr, L. Mayr, Q. Zhao, S. Soisuwan, B. Klötzer, S. Penner, ChemCatChem 5 (2013) 1273–1285.
[29] J.M. Gatica, R.T. Baker, P. Fornasiero, S. Bernal, J. Kaspar, J. Phys. Chem. B 105 (2001) 1191–1199.
[30] N. Iwasa, N. Ogawa, S. Masuda, N. Takezawa, Bull. Chem. Soc. Jpn. 71 (1998) 1451–1455.
[31] A.L. Bonivardi, M.A. Baltanás, J. Catal. 138 (1992) 500–517.
[32] S. Bernal, J.J. Calvino, M.A. Cauqui, J.M. Gatica, C. Larese, J.A. Pérez-Omil, J.M. Pintado, Catal. Today 50 (1999) 175–206.
[33] L. Kepinski, M. Wolcyrz, Appl. Catal. A: Gen. 150 (1997) 197–220.
[34] B.P. Burroughs, A. Hamnett, A.F. Orchard, G. Thornton, J. Chem. Soc. Dalton Trans. (1975) 1686–1698.
[35] A. Laachir, V. Perrichon, A. Badri, J. Lamotte, E. Catherine, J.C. Lavalley, J. El Fallah, L. Hilaire, F. Le Normand, E. Quéméré, G.N. Sauvion, O. Touret, J. Chem. Soc. Faraday Trans. 87 (1991) 1601–1609.
[36] A. Bayer, K. Flechtner, R. Denecke, H.-P. Steinrück, K.M. Neyman, N. Rösch, Surf. Sci. 600 (2006) 78–94.
[37] K. Dumbuya, R. Denecke, H.-P. Steinrück, Appl. Catal. A: Gen. 348 (2008) 209–213.
[38] C.D. Wagner, W.M. Riggs, L.E. Davis, J.F. Moulder, G.E. Muilenberg, Handbook of X-ray Photoelectron Spectroscopy, in: Perkin-Elmer (Ed.), Eden Praire, MN, 1978.
[39] W. Stadlmayr, C. Rameshan, C. Weilach, H. Lorenz, M. Hävecker, R. Blume, D. Rocha, Teschner, A. Knop-Gericke, D. Zemlyanov, S. Penner, R. Schlögl, G. Rupprechter, B. Klötzer, N. Memmel, J. Phys. Chem. C 114 (2010) 10850–10856.
[40] S. Liu, K. Takahashi, K. Fuchigami, K. Uematsu, Appl. Catal. A: Gen. 299 (2006) 58–65.
[41] G. Schön, J. Electron. Spectrosc. Relat. Phenom. 2 (1973) 75–86.
[42] E. Antonides, E.C. Janse, G.A. Sawatzky, Phys. Rev. B 15 (1977) 1669–1679.
[43] N. Takezawa, N. Iwasa, Catal. Today 36 (1997) 45–96.
[44] G. Avgouropoulos, J. Papavasiou, T. Ioannides, Chem. Eng. J. 15 (2009) 274–280.
[45] E.S. Ranganathan, S.K. Bej, L.T. Thompson, Appl. Catal. A: Gen. 289 (2005) 153–162.
[46] R.J. Gorte, S. Zhao, Catal. Today 104 (2005) 18–24.
[47] T. Bunluesin, R.J. Gorte, G. Graham, Appl. Catal. B: Environ. 15 (1998) 107–114.
[48] A.M. Karim, T. Conant, A. Datye, Phys. Chem. Chem. Phys. 10 (2008) 5584–5590.
[49] K.H. Lim, Z.X. Chen, K.N. Neyman, N. Rösch, J. Phys. Chem. B 110 (2006) 14890–14897.
[50] A. Haghofer, K. Föttinger, F. Girgsdies, D. Teschner, A. Knop-Gericke, R. Schögl, G. Rupprechter, J. Catal. 286 (2012) 1–9.
[51] C. Barrios, M.A. Baltanás, A.L. Bonivardi, Methanol steam reforming reaction on highly stable, ceria supported Pd/Zn-based catalysts, in: 15th. Intl. Congr. Catal. (15th. ICC), Munich (Germany), July 1–6, 2012, P 1.05_1795.
[52] N. Iwasa, M. Yoshikawa, W. Nomura, M. Arai, Appl. Catal. A: Gen. 292 (2005) 215–222.
[53] Y. Suwa, S. Ito, S. Kameoka, K. Tomishige, K. Kunimori, Appl. Catal. A: Gen. 267 (2004) 9–16.
[54] J. Papavasiliou, G. Avgouropoulos, Appl. Catal. B: Environ. 69 (2007) 226–234.
[55] L. Mo, X. Zheng, C.-T. Yeh, Chem. Phys. Chem. 6 (2005) 1470–1472.
[56] M. Boucher, N. Yi, F. Gittleson, B. Zugic, H. Saltsburg, M. Flytzani-Stephanopoulos, J. Phys. Chem. C 115 (2011) 1261–1268.